Resistance of A Marine Train

Zhi-Ming Yuan, Fengshen Zhu, Saishuai Dai

Dep. of Naval Architecture, Ocean & Marine Engineering, University of Strathclyde, Glasgow, G4 0LZ, UK

E-mail Address of the presenting author: zhiming.yuan@strath.ac.uk

1 INTRODUCTION

The rationale behind ducklings following their mother to swim in a single-file formation has been unveiled by Yuan et al. [1], shedding light on the phenomenon from the perspective of wave-riding and wave-passing. Drawing inspiration, Zhu et al. [2] explored ships in a single-file configuration and discovered that wave-passing can be achieved with ships maintaining an uniform separation. Figure 1 shows the wave patterns of an optimal ship formation. The waves generated by the leading ship are passed by its trailer, and then identical waves are maintained behind each ship. By repeating this process, the wave energy originating from the leading ship eventually reaches the last trailing ship.

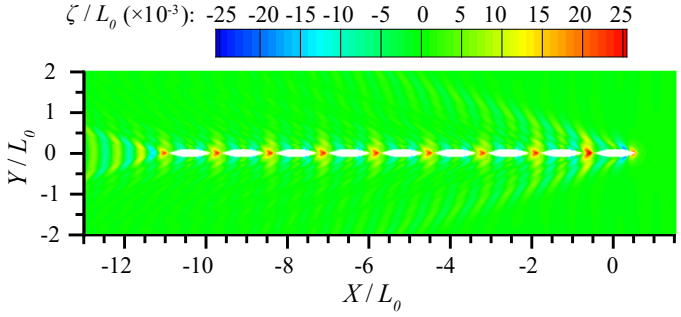

Figure 1 Wave patterns of an optimal ship formation.

In addition to utilizing wave interference to reduce resistance, the trailing ships may exploit other interferences, such as bubbles or turbulence flow in the wake of a leading ship, to save energy. Motivated by these interesting phenomena, some critical questions are raised:

- Can we quantify the contributions of wave interference and viscous interference to the total resistance reduction?
- How much resistance reduction in total can be achieved for formations with different configurations when considering the viscous effect?
- Does the transom stern design more effectively contribute to resistance reduction in ship formations compared to other stern designs?
- What role does the bubble flow generated by a leading ship play in reducing the resistance of a trailing ship?

The objective of this work is to explore the answers to the above questions.

2 EXPERIMENTAL SET-UP

A series of resistance tests were conducted in the towing tank at the Kelvin Hydrodynamics Laboratory (KHL), University of Strathclyde. Three distinct models were employed in the experiment, namely Model A, B and C. Model A is a rectangular box of 1m long, 0.25 m wide and 0.15 draft. A triangular prism of 0.25 side length is added to Model B at its bow, and the same triangular prism is added at the stern of Model C, as shown in Figure 2 (a).

Three distinct ship formations (Configuration I, II, and III) were investigated by incorporating various models, as illustrated in Figure 2 (a). Due to the adjustment range limitations of the sliding frame, the gap between the two models in Configuration I ranges from 0.1 m to 2.5 m. For Configuration II, the gap varies from 0.1m to 2.3 m, while for Configuration III, it extends from 0 m to 2 m. Given the

intensification of interference between the two models at closer separation distances, the initial adjustment interval is set to 0.05 m. As the distance between the models increases, this interval is adjusted to 0.1 m or more. The maximum testing speed is limited to avoid the impact of "green water". In ship formation tests, the movement speeds were set at 1.036 m/s, 1.209 m/s, 1.382 m/s, 1.554 m/s, 1.727 m/s, and 1.9 m/s, which correspond to Froude numbers of 0.3, 0.35, 0.4, 0.45, 0.5, and 0.55 for Model B, respectively.

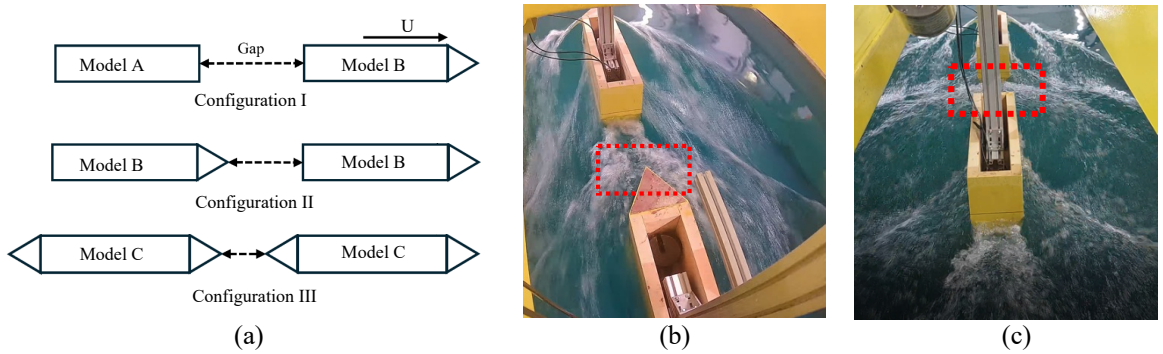

Figure 2 (a) Ship models and configurations in tank testing; (b) Wave field for Configuration II with G/L_0 = 0.5 at a velocity of 1.9 m/s; (c) Wave field for Configuration I with G/L_0 = 0.5 at a velocity of 1.727 m/s.

To quantify the hydrodynamic interactions, we define the resistance reduction coefficient as

$$C_{DR}^{T} = \left(1 - \frac{R_n^T}{R_S^T}\right) \times 100\%, n = 0, 1, 2, \ldots \quad (1)$$

where R_S^T is the total resistance of a single ship, either the leading one (n=0) or the trailing ones (n=1, 2, 3, …), moving solely in clam water; while R_n^T is the total resistance of a ship moving in a certain position in a formation with the presence of the other ships. Obviously, $C_{DR}^{T} > 0$ indicates the total resistance is reduced in a formation due to the hydrodynamic interaction; whilst $C_{DR}^{T} < 0$ represents an increase in total resistance. No interaction is found at $C_{DR}^{T} = 0$, and the total resistance is the same as that of independent moving.

3 RESULTS AND DISCUSSIONS

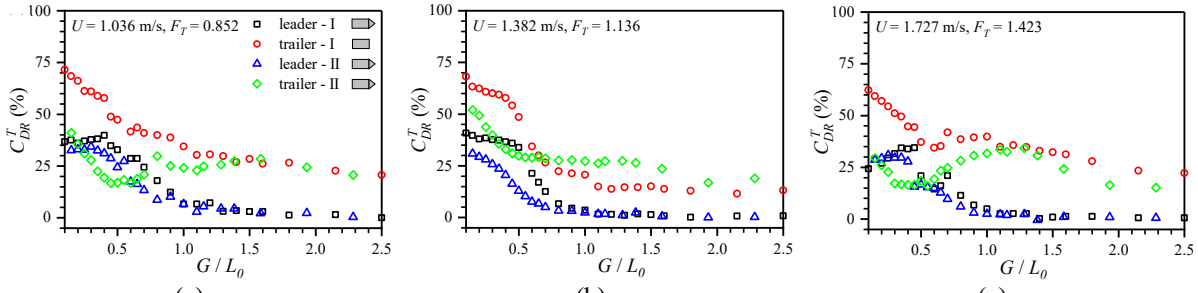

Figure 3 (a) Total drag reduction between Configurations I and II. (a) 1.036 m/s; (b) 1.382 m/s; (c) 1.727 m/s.

Figure 3 shows the reduction in total resistance for each ship in Configuration I and II across various speeds. When the gap G/L_0 (G is the gap and L_0 is the ship length of Model B) is less than 0.5, the C_{DR}^{T} values for both the leading and trailing ships in Configuration I are generally higher than those in Configuration II. Especially, the trailing ship in Configuration I consistently achieves a significant total resistance reduction, reaching approximately 70% at most speeds when the gap is very small. As the gap G/L_0 widens from 0.1 to 0.5, the C_{DR}^{T} values for the leading ship in Configuration II decrease more significantly than those in Configuration I. Understanding the wake field of a single ship with a transom stern is beneficial for analyzing the hydrodynamic interference between ships. The wake field of a transom stern can be segmented into three distinct regions along the flow direction: the converging wave corner region, the rooster tail region, and the divergent wave region, as shown in Figure 4 (a).

The flow separation behind the transom stern leads to stern ventilation, resulting in a nearly dry stern state. A hollow is observed behind the transom stern, with ridges rising from the lower corner. These ridges angle toward the stern centerline, entraining some air and generating significant spray. As the wake spreads laterally, the divergent wave train maintains a steady V-shape. Due to air entrainment and turbulent disturbance, a "whitewater zone" with numerous bubbles forms within the surrounding flow field (see Figure 2 (b), Figure 4 (c)&(d)). The trailing ship with a flat bow in Configuration I generates more frontal waves compared to the trailing ship with a sharp bow in Configuration II. These waves can fill the cavity behind the transom stern of the leading ship, significantly decreasing the hydrostatic resistance of the leading ship. In addition, a flat bow more effectively prevents cross flow from concentrating at the centre, thereby avoiding wave overturning and breaking. Additionally, it better utilizes the low-pressure area in the cavity region to reduce the stagnation pressure on the bow surface compared to a sharp bow.

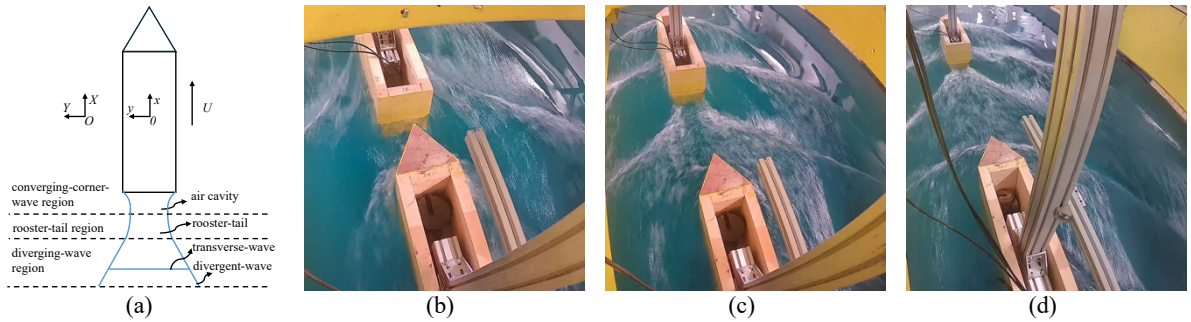

(a) (b) (c) (d)

Figure 4 (a): Characteristics of the wake filed behind a transom stern. (b), (c) & (d): The flow fields of three different gaps in Configuration II when the velocity is 1.554 m/s. (b) G/L_0 = 0.15; (c) G/L_0 = 0.7; (d) G/L_0 = 1.6.

The turning point of the C_{DR}^T values for the trailing ship in Configuration II is observed when G/L_0 is approximately 0.5. At this point, the bow of the trailing ship enters the high-pressure zone in the rooster tail region of the leading ship, which is unfavourable for resistance reduction. However, this effect is insignificant for the trailing ship in Configuration I, as the bow waves from the trailing ship prevented the formation of the rooster tail. Figure 2 (b) shows the wave field of Configuration II when the ships travel at a speed of 1.9 m/s with G/L_0 = 0.5. It is clear that the bow of the trailing ship is precisely positioned within the rooster tail region, where significant spray occurs due to the closure of the air cavity, resulting in a high-pressure zone. In Configuration II, the bow waves produced by the trailing ship are relatively weak and fail to disrupt the high-pressure rooster tail effectively. In contrast, as shown in Figure 2 (c), for Configuration I at a speed of 1.727 m/s with the same gap, the trailing ship with its flat bow generates stronger bow waves. These bow waves interfere with the closure of the air cavity flow, preventing the formation of the concentrated high-pressure rooster tail region. As a result, the adverse resistance effect on the trailing ship is mitigated.

When the gap G/L_0 exceeds 0.5, the C_{DR}^T values for the trailing ship in Configuration II gradually increase, with wave interference beginning to dominate the interaction between the two ships in the diverging wave region of the leading ship. The wave interference between the two ships becomes more intensive as speed increases. At higher speeds, the wave amplitude increases significantly, resulting in the C_{DR}^T values of the trailing ship following a sinusoidal wave like pattern, as illustrated in Figure 3 (c).

As the gap increases further, it becomes challenging for the leading ship to receive benefits from the interference, and the C_{DR}^T values for the leading ship in both configurations gradually approach zero. Simultaneously, the wave interference between the two ships weakens, and the C_{DR}^T values for the trailing ships in both configurations converge to constant values when G/L_0 exceeds 2 across various speeds. Within the turbulent-bubble mixed flow region, the resistance reduction primarily arises from the decrease in form resistance, as flow separation around the bow and behind the transom stern of the trailing ship is weakened when moving within the turbulent flow generated by the leading ship. This is analogous to the phenomenon where free-stream turbulence can shorten the separation bubble in a wind tunnel [3]. Additionally, resistance reduction is also achieved through a decrease in skin friction. When the trailing ship moves within the bubble flow, the local average fluid density and relative flow velocity

are both decreased compared to moving independently. The microbubbles may also enter the turbulent boundary layer near the hull surface, reducing the shear force.

Figure 4 (b), (c) and (d) illustrates the flow fields for three typical gaps at a speed of 1.554 m/s in configuration II. At G/L_0 = 0.15, both the leading and trailing ships experience reduced hydrostatic resistance. The transom ventilation of the leading ship is nearly eliminated, and the frontal waves generated by the trailing ship are minimal. When the gap G/L_0 increases to 0.7, the trailing ship enters the divergent wave zone, benefiting from wave interference between the two ships and significantly contributing to total resistance reduction. As the gap G/L_0 widens to 1.6, wave interference weakens, making the reduction in form resistance and frictional resistance the dominant factor in the total resistance reduction. These three positions represent different zones where the mechanisms contributing to total resistance reduction vary. It should be noted that the lengths of these zones depend on the moving speed, so there are no absolute boundaries, especially for the length of the wave-interference-dominated zone.

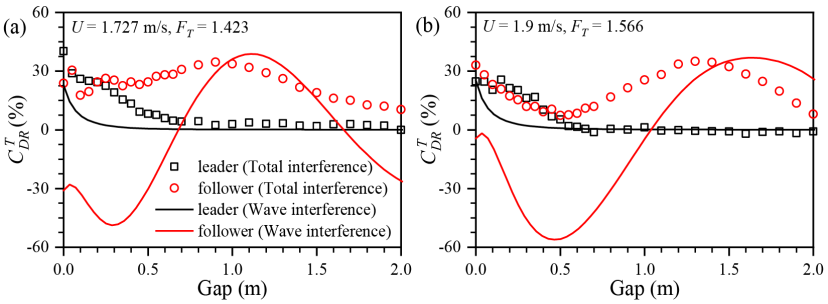

Figure 5 Total drag reduction between experimental and numerical results in Configuration III. (a) 1.727 m/s; (b) 1.9 m/s.

Figure 5 illustrates the reduction in total resistance measured in experiments and the wave resistance calculated by a linear potential flow solver MHydro for each individual in Configuration III. When the gap G/L_0 is less than 0.5, the resistance reduction values due to total interference for the leading ship are greater than those caused by wave interference alone. Additionally, as the gap widens, the wave resistance reduction for the leading ship decreases more rapidly compared to the total resistance reduction. Within potential flow theory, flow separation due to viscosity is not considered. In the real world, energy loss due to flow separation is unavoidable, especially for bluff bodies. In the experiments, the frontal waves generated by the trailing ship can not only reduce wave resistance by offering a propulsion force for the leading ship but also help mitigate flow separation, thereby reducing viscous resistance. When the gap G/L_0 exceeds 0.5, the wave interference C_{DR}^T (without viscous effect) of the leading ship is almost identical to the total C_{DR}^T (considering the viscous effect). This is because the frontal waves from the trailing ship can no longer reach the stern of the leading ship, making it challenging to alter the wave field around the leading ship.

The wave resistance reduction values of the trailing ship oscillate around zero, while the total resistance reduction values of the trailing ship oscillate around a positive value. Thus, the resistance reduction due to viscous interference varies nearly linearly, with a slow decrease as the distance increases. This suggests that the trailing ship periodically benefits from wave interference while consistently gaining from viscous interference when moving in the turbulent flow of the leading ship. There is a phase difference between the total resistance reduction and the wave resistance reduction because the wave patterns are influenced by the turbulent disturbance, which further impacts the wave interference between the two ships.

4 REFERENCES

[1] Z.-M. Yuan, M. Chen, L. Jia, C. Ji, and A. Incecik, 2021. *Wave-riding and wave-passing by ducklings in formation swimming*. J. Fluid Mech., 928, R2.
[2] F. Zhu, and Z.-M. Yuan, 2024. *Wave drag and wave patterns by ships moving in a single-file formation*. Phys. Fluids, 36.
[3] Y. Nakamura, and S. Ozono, 1987. *The effects of turbulence on a separated and reattaching flow*. J. Fluid Mech., 178, 477 (1987).